RSC Advances

ROYAL SOCIETY OF CHEMISTRY

www.rsc.org/advances

RSC Advances

PAPER

Synthesis and characterization of 2,2'-bithiophene end-capped dihexyloxy phenylene pentamer and its application in solution-processed organic ultraviolet photodetector

Received 00th May 2016,
Accepted 00th May 2016

DOI: 10.1039/x0xx00000x

www.rsc.org/

Lih Wei Lim*[a], Chin Hoong Teh[b], Rusli Daik[c], Norazilawati Muhamad Sarih[d], Mohd Asri Mat Teridi[b], Fahmi Fariq Muhammad[e], Khaulah Sulaiman*[a]

In this work a new solution processable small organic material, namely 2,2'-Bithiophene end-capped dihexyloxy phenylene pentamer ($BHBT_2$) was synthesized, characterized and applied in the fabrication of organic ultraviolet photodetector. The material was synthesized via Williamson etherification, bromination and Suzuki coupling. FTIR and NMR spectroscopies were recorded for the $BHBT_2$ along with its optical, thermal and electrochemical properties. Finally, the $BHBT_2$ was used as donor material to produce a solution-processed UV photodetector based on $BHBT_2$:$PC_{61}BM$ organic active layer. Results showed that in the forward biasing, the photodetector exhibited photovoltaic effect with Jsc = 1.80 mA, Voc = 0.66 V, FF = 0.30 and PCE = 0.98 %, while in the reverse biasing, the photodetector exhibited fast, reversible and stable response with the highest detectivity of 1.47×10^9 Jones. The realization of efficient UV detection was attributed to the strong absorption of $BHBT_2$ and $PC_{61}BM$ in the UV region. Hence, $BHBT_2$ pentamer coupled with $PC_{61}BM$ can be considered as potential materials to be applied in the solution-processed organic UV photodetector.

Introduction

Organic materials have received considerable attention for their employment, as promising alternatives to the inorganic materials, in the development of optoelectronics devices.[1-5] Along this line, inorganic based ultraviolet (UV) photodetectors are the most common devices used in the field of environmental monitoring, medicine, missile plume detection and solar astronomy.[6, 7] In spite of the wide application of UV photodetectors, their production is cumbersome due to the high cost and complexity involved in the materials processing and fabrication techniques. In recent years, organic semiconductors were successfully applied in the fabrication of UV photodetectors (PDs), by which a light weight, colour selective, and flexible device can be realized.[8-14] Besides, the comparable detectivity of organic UV photodetectors to that of the inorganic ones has granted organic based UV detectors great attraction in both academic and industrial scopes. Both small molecules and polymers have been employed as the active layer for UV PDs. Gong and coworkers used low bad gap semiconducting polymer, PDDTT blended with $PC_{60}BM$ to fabricate organic photodetector with a broad spectral response from 300 to 1450 nm.[10] Liu et al. demonstrated organic UV photodetectors with high response under illumination of 365 nm UV light by using 4,4',4"-tri-(2-methylphenyl phenylamino) triphenylaine (m-MTDATA) and two phosphorescent Cu(I) complexes.[15] In addition, Wu et al. found that photodetectors based on m-MTDATA: 4,7-diphenyl-1,10-phenanthroline-(bathophenanthroline) (Bphen) can be operated at deep UV region (< 300nm) through concealing the UV light longer than 300 nm through applying N,N'-diphenyl-N,N'-bis(3-methyl-phenyl)(1,1'-biphenyl)-4,4'-diamine (TPD) layer.[11] Wang et al. have utilized poly(N-vinyl carbazole):[6,6]-phenyl-C_{71}-butyric acid methyl ester (PVK:$PC_{71}BM$) to fabricate their inverted structure organic UV photodetector.[16] Evidently, small molecular organic semiconductors are famous for their enhanced charge carrier transport over that of the large molecular organics (organic polymers), and their employment in UV PDs was acted upon improving the performance of the devices. Su et al. fabricated devices by utilizing vacuum evaporation technique that showed high detectivity in the order of 10^{12} Jones from visible to near infrared regions, which is among the highest detectivities reported for organic small molecule PDs.[1] The main problem remains in front of the vast application of small molecular organics in photodetectors is the lack of their solution processability in organic solvents.

Most research literatures have shown that the UV photodetectors were fabricated from the solution processable

*Corresponding author
[a] Low Dimensional Materials Research Centre, Department of Physics, University of Malaya, 50603 Kuala Lumpur, Malaysia. E-mail: lihwei_lim@hotmail.com, khaulah@um.edu.my; Fax: +603-79674146; Tel: +603-79674087
[b] Solar Energy Research Institute, Universiti Kebangsaan Malaysia, 43600 UKM Bangi, Selangor, Malaysia.
[c] School of Chemical Sciences and Food Technology, Faculty of Science and Technology, Universiti Kebangsaan Malaysia, 43600 UKM Bangi, Selangor, Malaysia.
[d] Department of Chemistry, Faculty of Science, University of Malaya, 50603 Kuala Lumpur, Malaysia.
[e] Soft Materials and Devices Lab, Department of Physics, Koya University, Koya, Kurdistan Region, Iraq.

inorganic materials and organic polymers. However, synthesis and application of solution processable small organic molecules based UV photodetectors have not been widely reported. Hence, this research work was devoted to synthesize and characterize a new solution processable small molecular organic donor that is capable of absorbing UV light and to be applied in the UV photodetector. The small organic material was synthesized through Williamson etherification, bromination and Suzuki coupling reactions, and named as 2,2'-bithiophene end-capped dihexyloxy phenylene ($BHBT_2$) pentamer. The advantages of possessing efficient UV absorption and good adhesion to the substrate, due to the presence of dihexyloxy phenylene moiety, were also preserved along with its high solubility in the organic solvents; these are without affecting the electronic properties of the pentamer itself. Consequently, the spectroscopic, optical, thermal and electrochemical properties of $BHBT_2$ pentamer are reported. This $BHBT_2$ pentamer is later applied as donor material and mixed with $PC_{61}BM$ to fabricate solution-processed bulk heterojunction UV photodetectors. $PC_{61}BM$ is selected as acceptor material due to its high mobility and high absorption in the UV region. In addition, $PC_{61}BM$ can be also dissolved in the same organic solvents used to dissolve $BHBT_2$, such as chloroform and dichlorobenzene. Therefore, both $PC_{61}BM$ and $BHBT_2$ were prepared in solution-processable bulk heterojunction structure. To the best of our knowledge, this is the first work reports on the spectroscopic, optical, thermal and electrochemical investigations of $BHBT_2$ pentamer and its UV detection related properties in the $BHBT_2$:$PC_{61}BM$ bulk heterostructure. The fabricated devices showed decent PV effects under forward bias condition as well as fast, reversible and stable UV detection response in reverse bias.

Experimental

Materials and synthesis procedures

Reagent grade tetrahydrofuran (THF) and dimethylformamide (DMF) were distilled according to the work reported elsewhere.[17] Williamson etherification and Suzuki coupling reactions were carried out under nitrogen atmosphere. 2-Thiophene boronic acid and tetrakis(triphenylphosphine) palladium(0), ($Pd(PPh_3)_4$) were purchased from Acros Organics. Meanwhile, [6, 6]-Phenyl-C_{61} butyric acid butyl ester ($PC_{61}BM$) with purity >99 % was obtained from Sigma Aldrich and poly(3,4-ethylenedioxythiophene):poly(styrene sulfonate) (PEDOT:PSS) aqueous solution with conductivity of 900-1000 Scm^{-1} was purchased from H.C. Starck. All reagents were used as received unless otherwise specified.

Synthesis of 1,4-bis(hexyloxy)benzene (1). A solution of 1-bromohexane (0.19 mol) in DMF was added stepwise to a stirred solution of hydroquinone (10.00 g, 90.82 mmol) and potassium carbonate (26.38 g, 0.19 mol) in DMF at room temperature with dry N_2 inlet. The mixture was stirred at room temperature for 2 h, followed by heating under reflux at 100 °C overnight. The mixture was cooled to room temperature and then water was added. The aqueous solution was extracted with several portions of ethyl acetate and the combined organic extract was washed with water and brine. The organic extract was dried over anhydrous $MgSO_4$, and the solvent was evaporated. The crude product was further purified through silica gel column chromatography with hexane as eluent to afford the title compound **1** as white solid. Yield: 15.68 g (62 %). Mp: 45.0 – 47.0 ºC. IR (KBr, cm^{-1}): υ 3103, 3048 (υ_{CH}, Ph); 1511, 1476 (υ_{CC}, Ph); 1116 (δ_{CH}, ip, Ph); 828, 807 (δ_{CH}, oop, Ph); 2936, 2871 (υ_{CH}, O-CH_2); 1397 (δ_{CH}, O-CH_2); 1287, 1239, 1032 (υ_{COC}, Ph-O-CH_2); 534 (δ_{COC}, ip, Ph-O-CH_2); 2956 (υ_{CH}, CH_3); 1382 (δ_{CH}, CH_3); 1161, 1057 (υ_{CCC}, aliphatic); 945, 897 (δ_{CH}, CH_3); 772, 756(δ_{CH}, CH_2); ^{1}H NMR (400 MHz, $CDCl_3$, δ): 0.91 (t, *J*=6.8 Hz, 6H), 1.35 (m, 8H), 1.46 (m, *J*=7.1 Hz, 4H), 1.76 (m, *J*=7.2 Hz, 4H), 3.91 (t, *J*=6.6 Hz, 4H), 6.83 (s, 4H); ^{13}C NMR (400 MHz, $CDCl_3$, δ): 14.2, 22.8, 26.0, 29.6, 31.8, 68.9, 115.6, 153.4. MS (EI): m/z calculated for $C_{18}H_{30}O_2$, 278.4; found 278.2$[M]^+$.

Synthesis of 2,5-dibromo-1,4-bis(hexyloxy)benzene (2). In a three neck round bottom flask, a glacial acetic acid solution of 1,4-bis(hexyloxy)benzene **1** (20.00 mmol) was added dropwise into a solution of Br_2 (6.71 ml, 42.00 mmol) in glacial acetic acid. The mixture was stirred at room temperature for 2 h, followed by heating under reflux at 40 ºC for 2 h. The mixture was cooled to room temperature and then quenched with water. The crude product was collected by filtration and washed thoroughly with water and 1 M sodium bicarbonate solution. The crude product was recrystallized twice with ethyl acetate-ethanol to give the title compound **2** as colorless crystals. Yield: 8.20 g (94 %). Mp: 62.0 – 64.0 ºC. IR (KBr, cm^{-1}): υ 1494, 1460 (υ_{CC}, Ph); 1125 (δ_{CH}, ip, Ph); 849, 829, 806 (δ_{CH}, oop, Ph); 440 (δ_{CC}, Ph); 2938, 2869 (υ_{CH}, O-CH_2); 1396 (δ_{CH}, O-CH_2); 1270, 1210, 1022 (υ_{COC}, Ph-O-CH_2); 526 (δ_{COC}, ip, Ph-O-CH_2); 2956, 2851 (υ_{CH}, CH_3); 1360 (δ_{CH}, CH_3); 1166, 1060 (υ_{CCC}, aliphatic); 901 (δ_{CH}, CH_3); 754 (δ_{CH}, CH_2); 635 (υ_{CBr}, Ph-Br); ^{1}H NMR (400 MHz, $CDCl_3$, δ): 0.92 (t, *J*=7.1 Hz, 6H), 1.35 (m, 8H), 1.49 (m, *J*=7.4 Hz, 4H), 1.81 (m, *J*=7.1 Hz, 4H), 3.95 (t, *J*=6.6 Hz, 4H), 7.09 (s, 2H); ^{13}C NMR (400 MHz, $CDCl_3$, δ): 14.2, 22.8, 25.8, 29.3, 31.7, 70.6, 111.4, 118.7, 150.3. MS (EI): m/z calculated for $C_{18}H_{28}Br_2O_2$: 436.2; found 436.0$[M^+]$.

Synthesis of 1,4-bis(thiophen-2-yl)-2,5-dihexyloxybenzene (3). $Pd(PPh_3)_4$ (0.28 g, 0.24 mmol) and anhydrous Na_2CO_3 solution (2M, 15 ml, 30.00 mmol) were added to a solution of 2,5-dibromo-1,4-bis(hexyloxy)benzene **2** (4.00 mmol) in THF at room temperature with a slow dynamic flow of dry N_2 gas. A solution of 2-thiophene boronic acid (1.54 g, 12.00 mmol) in THF were prepared and then syringed into the reactor. The mixture was degassed with dry N_2 gas for 30 min prior to heating under reflux at 58 °C for 24 h. Water was added to neutralize the mixture after the reaction chilled to room temperature. The aqueous solution was extracted with several portions of dichloromethane and the isolated organic extract was washed with water and brine. It was later dried over anhydrous $MgSO_4$ and the solvent was removed. The residue was further purified through silica gel column chromatography with hexane-

dichloromethane (v/v=9:1) as eluent and recrystallization in ethyl acetate-ethanol to yield the coupled product **3** as pale yellowish needle crystals. Yield: 1.42 g (80.0%). mp: 94.0 – 96.0 ºC. IR (KBr, cm^{-1}): υ 3093, 3069 (υ_{CH}, Th); 1533, 1429, 1403, 1343 (δ_{CC}, ip, Th); 742, 725, 694 (δ_{CH}, oop, Th); 682 (υ_{CS}, Th); 497 (δ_{CC}, oop, Th); 1584, 1489, 1471 (υ_{CC}, Ph); 1262, 1126 (δ_{CH}, ip, Ph); 856, 818, 802 (δ_{CH}, oop, Ph); 440 (δ_{CC}, Ph); 2949, 2869 (υ_{CH}, O-CH_2); 1393 (δ_{CH}, O-CH_2); 1284, 1220, 1035 (υ_{COC}, Ph-O-CH_2); 526 (δ_{COC}, ip, Ph-O-CH_2); 2964, 2884 (υ_{CH}, CH_3); 2918, 2852 (υ_{CH}, CH_2); 1359 (δ_{CH}, CH_3); 1163, 1069(υ_{CCC}, aliphatic); ^{1}H NMR (400 MHz, $CDCl_3$, δ): 0.93 (t, *J*=7.2 Hz, 6H), 1.39 (m, 8H), 1.56 (m, *J*=7.5 Hz, 4H), 1.91 (m, *J*=7.1 Hz, 4H), 4.10 (t, *J*=6.6 Hz, 4H), 7.11 (t, *J*=3.6 Hz, *J*=5.4 Hz, 2H), 7.35 (d, *J*=5.4 Hz, 2H), 7.55 (d, *J*=3.6 Hz, 2H); ^{13}C NMR (400 MHz, $CDCl_3$, δ): 14.0, 22.6, 25.9, 29.4, 31.6, 69.8, 113.0, 123.1, 125.2, 125.6, 126.7, 139.3, 149.3. MS (ESI, positive): m/z calculated for $C_{26}H_{34}O_2S_2 + K^+$: 481.6; found 481.1 $[M+K]^+$.

Synthesis of 1,4-bis(5-bromo-thiophen-2-yl)-2,5-dihexyloxybenzene (4). To a solution of 1,4-bis(thiophen-2-yl)-2,5-dihexyloxybenzene, **3** (2.00 mmol) in THF was added N-bromosuccinimide (NBS) (0.72 g, 4.02 mmol). The reaction was conducted in dark with a continuous flow of N_2 gas. The mixture was stirred at room temperature for 4 h before water was added to quench the reaction. The aqueous solution was extracted with portions of dichloromethane. The organic extracts were combined, washed with water and brine. It was then dried over anhydrous $MgSO_4$ and the solvent was removed. The crude product was recrystallized twice with hexane-dichloromethane (v/v=9:1) to yield the title compound **4** as yellowish crystals. Yield: 0.98 g (81.7%). Mp: 106.0 – 108.0 ºC. IR (KBr, cm^{-1}): υ 3105, 3074 (υ_{CH}, Th); 1539, 1432, 1403 (δ_{CC}, ip, Th); 724, 696 (δ_{CH}, oop, Th); 686 (υ_{CS}, Th); 495, 466(δ_{CC}, oop, Th); 658 (υ_{CBr}, Th-Br); 1493, 1474, 1468 (υ_{CC}, Ph); 1267, 1127 (δ_{CH}, ip, Ph); 848, 802, 786 (δ_{CH}, oop, Ph); 441 (δ_{CC}, Ph); 2942, 2871 (υ_{CH}, O-CH_2); 1395 (δ_{CH}, O-CH_2); 1278, 1217, 1030 (υ_{COC}, Ph-O-CH_2); 554 (δ_{COC}, ip, Ph-O-CH_2); 2956 (υ_{CH}, CH_3); 2915, 2852 (υ_{CH}, CH_2); 1337 (δ_{CH}, CH_3); 1162, 1058 (υ_{CCC}, aliphatic); ^{1}H NMR (400 MHz, $CDCl_3$, δ): 0.94 (t, *J*=6.9 Hz, 6H), 1.39 (m, 8H), 1.53 (m, 4H), 1.92 (m, *J*=7.1 Hz, 4H), 4.08 (t, *J*=6.6 Hz, 4H), 7.05 (d, *J*=3.6 H, 2H), 7.17 (s, 2H), 7.25 (d, *J*=3.6 Hz, 2H); ^{13}C NMR (400 MHz, $CDCl_3$, δ): 14.0, 22.6, 25.9, 29.3, 31.6, 69.9, 111.5, 113.2, 122.6, 124.6, 129.3, 140.4, 149.0. MS (ESI,positive): m/z calculated for $[C_{26}H_{32}Br_2O_2S_2 + 2H]^{2+}$: 301.2; found 301.1 $[M+2H]^{2+}$.

Synthesis of 1,4-bis(2,2'-bithiophen-5-yl)-2,5-dihexyloxybenzene ($BHBT_2$). The synthesis of $BHBT_2$ pentamer was conducted according to the same procedures as the title compound **3** by using 2-thiophene boronic acid and 1,4-bis(5-bromo-thiophen-2-yl)-2,5-dihexyloxybenzene, **4**. The crude product was isolated through column chromatography on silica eluted with hexane-dichloromethane (v/v=9:1) followed by higher polarity of eluent (v/v=8:2) and (v/v=7:3). The isolated product was subsequently recrystallized in a mixture of hexane-dichloromethane to yield the coupled product, $BHBT_2$ pentamer as orange solid. Yield: 0.50 g (82.4%). Mp: 146.5 – 147.8 ºC. IR (KBr, cm^{-1}): υ 3114, 3065 (υ_{CH}, Th); 1514, 1402 (δ_{CC}, ip, Th); 748 (δ_{CH}, oop, Th); 689 (υ_{CS}, Th); 481 (δ_{CC}, Th); 1458 (υ_{CC}, Ph); 843, 795 (δ_{CH}, oop, Ph); 448 (δ_{CC}, Ph); 2947, 2856 (υ_{CH}, O-CH_2); 1272, 1206, 1040 (υ_{COC}, Ph-O-CH_2); 2919 (υ_{CH}, CH_2); 932 (δ_{CH}, CH_3); 1080 (υ_{CC}, aliphatic); ^{1}H NMR (400 MHz, $CDCl_3$, δ): 0.92 (t, *J*=7.1 Hz, 6H), 1.38 (m, 8H), 1.58 (m, 4H), 1.93 (m, *J*=7.1 Hz, 4H), 4.11 (t, *J*=6.6 Hz, 4H), 7.03 (t, *J*=3.7 Hz, *J*=3.7 Hz, 2H), 7.17 (d, *J*=3.7 Hz, 2H), 7.21 (d, *J*=2.9 Hz, 2H), 7.23 (d, *J*=2.9 Hz, 2H), 7.25 (s, 2H), 7.46 (d, *J*=3.7 Hz, 2H); ^{13}C NMR (400 MHz, $CDCl_3$, δ): 14.2, 22.7, 26.1, 29.5, 31.7, 69.9, 112.1, 122.8, 123.4, 123.6, 124.3, 125.9, 127.9, 137.4, 137.8, 138.2, 149.3. MS (ESI, positive): m/z calculated for $C_{34}H_{38}O_2S_4 + H^+$: 607.9; found 607.2 $[M+H]^+$.

Device Fabrication

A concentration of 20 mg/ml stock solution of $BHBT_2$:$PC_{61}BM$ with the weight ratio of 1:1 was made through dissolving $BHBT_2$ pentamer and $PC_{61}BM$ in HPLC grade chloroform. The $BHBT_2$:$PC_{61}BM$ solution was stirred overnight at room temperature. Both $BHBT_2$:$PC_{61}BM$ and PEDOT:PSS solutions were filtered respectively by using 0.20 µm and 0.45 µm nylon filter prior to use. ITO coated substrates (20 Ω/sq. sheet resistance from Ossila) were cleaned sequentially by using acetone, isopropanol, deionized water and finally blow-dried by using N_2 gases. Then, the ITO coated substrates were treated with 35 W oxygen plasma for 5 minutes in order to enhance the adhesion of PEDOT:PSS on the ITO surface .

For device fabrication, PEDOT:PSS solution was spun onto the ITO coated surface (anode) at spin rate of 4000 rpm (revolutions per minute) for 30 seconds to form a (38±3) nm thickness thin buffer layer. Then, the PEDOT:PSS buffer layer was annealed at 130 °C for 10 minutes to remove water residue. This was followed by the coating of $BHBT_2$:$PC_{61}BM$ solution at spin rate of 4000 rpm for 30 seconds to yield a homogenous thin film with thickness of (180.6±7.3) nm. Finally, the devices were completed by coating aluminium (Al) electrodes onto the active layer as cathodes under high vacuum (1×10^{-5} mbar) condition through thermal evaporating technique. The average thickness of the Al electrodes was about (83.7±19.2) nm. The ITO/PEDOT:PSS/$BHBT_2$:$PC_{61}BM$/Al devices were underwent post-deposition annealing at 80 °C for 10 minutes on a hot plate. All the device fabrication processes except thermal evaporation of Al were prepared under the ambient condition inside a 10 k clean room.

Characterization of Materials and Devices

The FTIR spectra of intermediate compounds and $BHBT_2$ pentamer in KBr pellets were recorded using a GX Perkin-Elmer Infrared Spectrometer in the range of 4000 to 370 cm^{-1}. (Abbreviations used: Ph, phenylene; Th, thiophene; ip, in-plane bending; oop, out of plane bending). ^{1}H and ^{13}C NMR spectra were obtained using a Jeol FT-NMR model ECP 400 MHz spectrometer with deuterated chloroform ($CDCl_3$) and tetramethylsilane (TMS) as solvent and internal standard respectively. (Abbreviations indicated: s, singlet; d, doublet; t, triplet; m, multiplet.). The mass spectra were measured with a GC/MSD configuration consisted of an Agilent

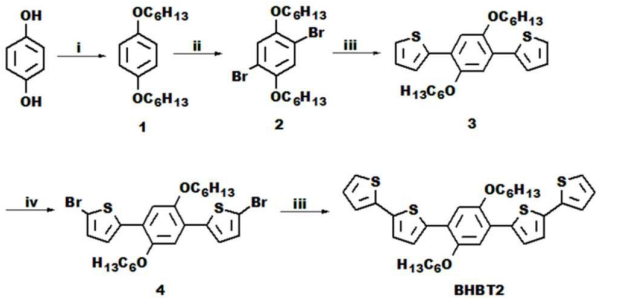

Reagents and conditions: (i) $C_6H_{13}Br$, DMF, K_2CO_3, reflux, 24 hrs; (ii) Br_2, CH_3COOH, rt, 2 hrs; (iii) 1. $Pd(PPh_3)_4$, 2M Na_2CO_3, THF, rt. 2. 2-thiophene boronic acid, THF, reflux, 24 hrs; (iv) NBS, THF, rt, 4 hrs

Scheme 1 Synthetic route for intermediate compounds and $BHBT_2$ pentamer.

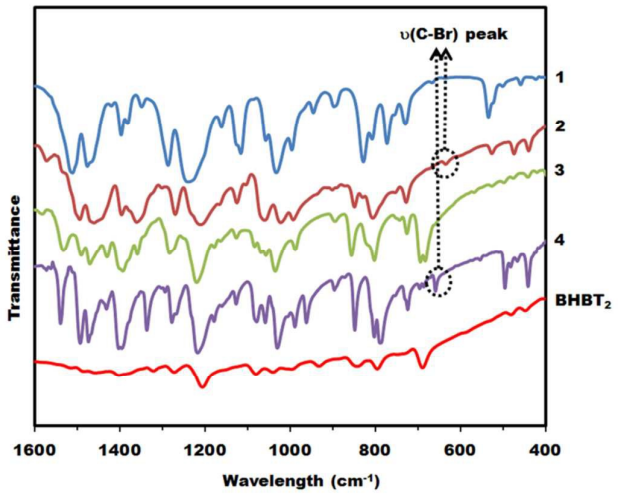

Fig.1 FTIR spectra of intermediate compounds 1, 2, 3, 4 and $BHBT_2$ pentamer.

7890A gas chromatograph (GC) directly coupled to the mass spectrometer system (MS) of an Agilent 5975C inert MSD with triple-axis detector (EI 70 eV, mass range 45-600 Da) or on a LC-MS-TOF Bruker MicroTOF-Q mass spectrometer with a MS direct infuse (ESI, mass range 100-800 Da) into a Dionex Ultimate 3000 liquid chromatography (LC). Melting points were determined on a Barnstead Electrothermal digital melting point apparatus model 1A 9100. The photoluminescence (PL) spectrum was measured in $CHCl_3$ solution by using Perkin Elmer LS55 spectrometer. The cyclic voltammograms were recorded on a Metrohm Autolab Potentiostats model Autolab PGSTAT12 at room temperature using saturated calomel electrode (SCE) as a reference electrode and two platinum wires as working and auxiliary electrode correspondingly in an electrolytic solution of 0.1 M tetrabutylammonium hexafluorophosphate, n-Bu_4NPF_6 in dry CH_2Cl_2 at a sweep rate of 100 mV/s. DSC analysis was performed on a Mettler Toledo model DSC 823e under static air with scanning rate ±10 °C/min. The heating–cooling cycle was repeated twice in the range of 25 °C to 200 °C. Thermal gravimetric analysis (TGA) of the $BHBT_2$ pentamer was carried out on a Mettler Toledo model TGA/STDA 851e over a temperature range of 30-600 °C under nitrogen atmosphere at a heating rate of 10 °C/min.

The thicknesses of the thin films were characterized by a KLA Tencor P-6 Surface profilometer. Perkin Elmer Lamda 950 UV-Vis-NIR spectrophotometer was used to record the UV-Vis absorption spectra of $BHBT_2$ in $CHCl_3$ solution and in solid state thin films. The current density-voltage (J-V) measurements were measured by using a Keysight B2902A Precision Source/Measure Unit. For photovoltaic studies, the devices were put under AM 1.5 G illumination with the light intensity of 36 mW/cm^2 provided by Newport Xenon Arc Lamp. Incident intensity of 36 mW/cm^2 was used instead of standard 100 mW/cm^2 because of the limitation of the Xenon arc lamp. Optical filter with difference optical density was used to adjust the light intensity from 3.6 mw/cm^2 to 36 mw/cm^2. Time response upon 36 mW/cm^2 light illumination was measured by a mechanical chopping method along with the Keysight B2902A Precision Source/Measure Unit. Fast response measurements were measured by using nitrogen laser pulse from Stanford Research Systems (SRS) NL100 which is able to provide 337 nm signals with 3 ns pulse width from the rate of 1 Hz to 20 Hz. The transient photocurrent of the photodetector was recorded by Agilent Technologies InfiniiVision D30-X 3052A Digital Storage Oscilloscope (500MHz 4GSa/s) with Agilent N2890A 10:1 Passive Probe (500MHz 10MΩ/11pF 300VRMS CAT I, II). In the EQE measurements, monochromatic light was supplied by Newport Oriel Apex Monochromator Illuminator. The intensity of the light sources was measured by using Newport Power Meter (Model 1918-R) together with the UV enhanced silicon photodetector (Model 818-UV).

Results and Discussion

Synthesis and spectroscopic studies

The synthetic route of soluble $BHBT_2$ pentamer is represented in Scheme 1. The introduction of hexyloxy chains was conducted on hydroquinone through Williamson etherification by using 1-bromohexane and K_2CO_3 in dry DMF, leading to 1,4-bis(hexyloxy)benzene **1** with moderate yield (62 %).[18] Subsequent bromination in a mixture of bromine in CH_3COOH afforded an excellent yield (94 %) of 2,5-dibromo-1,4-bis(hexyloxy)benzene **2** which is ready for Suzuki coupling reaction.[19] 1,4-bis(thiophen-2-yl)-2,5-dihexyloxybenzene, **3** (80 %) was obtained from coupling between 2-thiophene boronic acid with compound **2** in a solution of 2M Na_2CO_3 in THF with $Pd(PPh_3)_4$ as catalyst via Suzuki coupling.[20] Compound **3** was later subjected to bromination with NBS in THF at room temperature and obtained as 1,4-bis(5-bromo-thiophen-2-yl)-2,5-dihexyloxybenzene **4** in good yield (81.7 %). $BHBT_2$ pentamer is obtained as a result of coupling between compound **4** with 2-thiophene boronic acid reagents following Suzuki coupling procedures as reported for compound **3**. Further purification of the crude product in column chromatography on silica eluted with hexane-dichloromethane (v/v=9:1) followed by higher polarity of eluent (v/v=8:2) and (v/v=7:3) several times, afforded $BHBT_2$

RSC Advances

PAPER

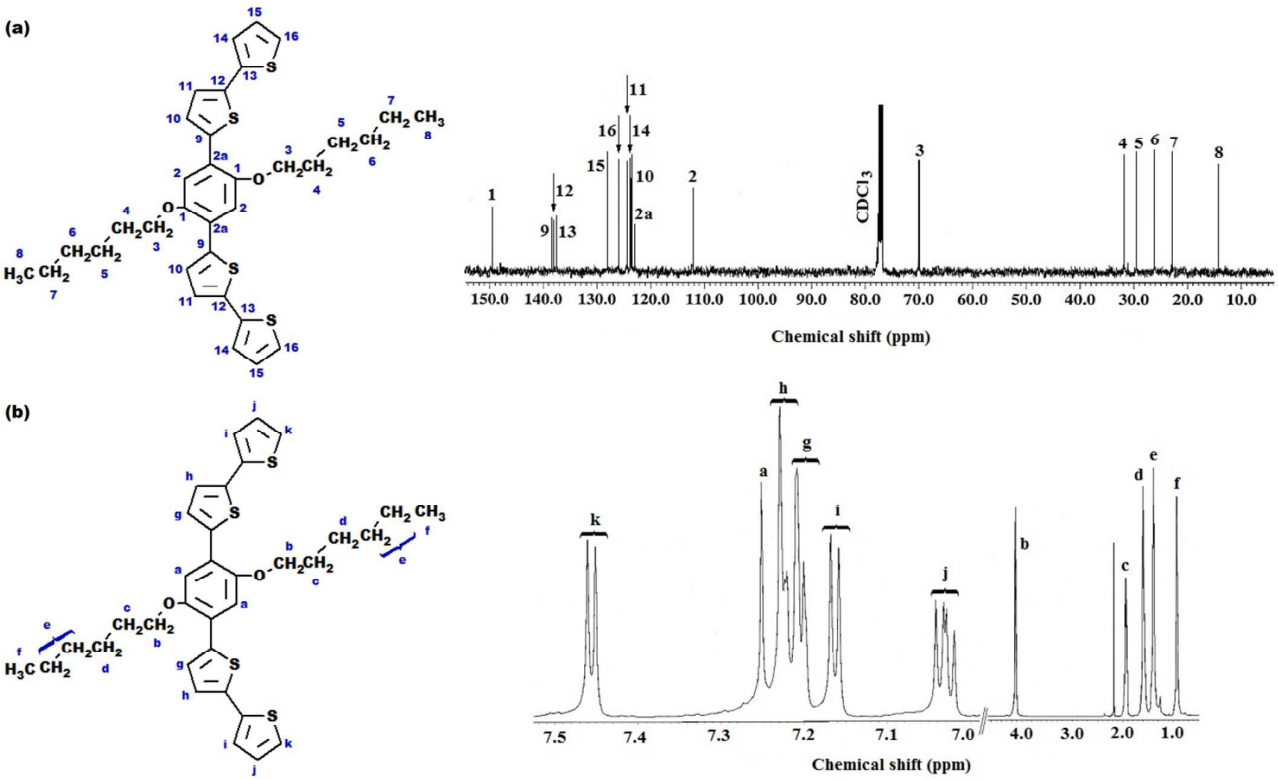

Fig. 2 (a) ^{13}C and (b) ^{1}H NMR chemical shifts and assignments of $BHBT_2$ pentamer.

Table 1 Solubility at room temperature, absorption maxima (λ_{abs}) and emission maxima (λ_{em}) in $CHCl_3$ solution, and thermal properties of $BHBT_2$ pentamer.

Solubility (g/L)			λ_{abs} [a]	λ_{em} [a]	T_m, T_c [b]	T_d [c]
$CHCl_3$	CH_2Cl_2	THF	(nm)	(nm)	(° C)	(° C)
59.00	42.46	88.76	344, 416*	467*, 496	149.7, 109.5	300

[a] absolute maximum is denoted by an asterisk (*)

[b] T_m and T_c were determined from the second cycle of DSC trace and defined as melting temperature and crystallization temperature, respectively

[c] T_d has been defined as thermal stability of the sample before weight loss started

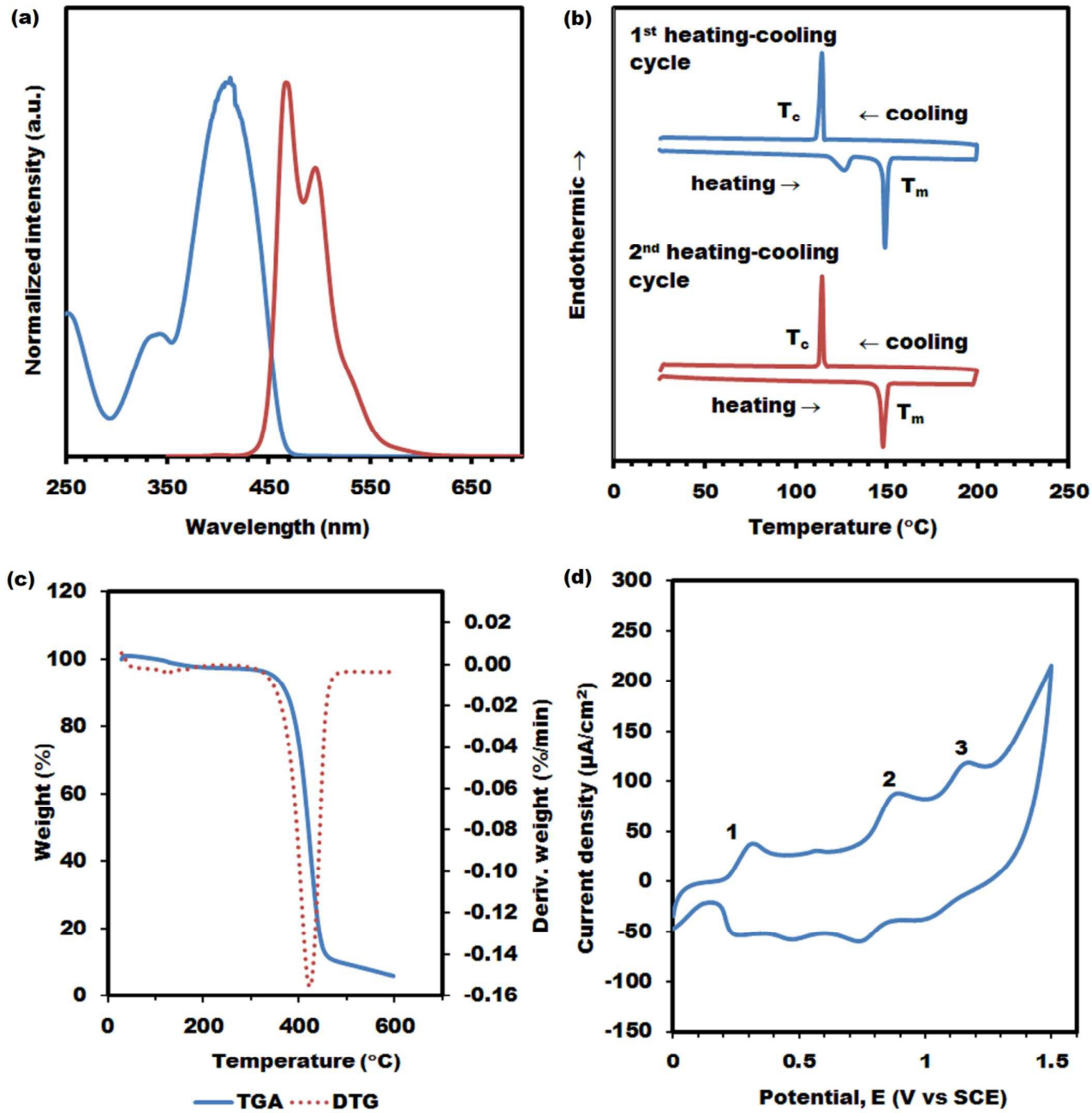

Fig. 3 Optical, thermal and electrochemical properties of $BHBT_2$ pentamer. (a) UV absorption (blue line) and emission (red line) spectra in $CHCl_3$ solution, (b) Repetitive heating-cooling cycles of DSC thermograms under static air with scanning rate ± 10 °C/min from 25-200 °C, (c) TGA (blue line) and DTG (red dots line) thermograms from 30 °C - 600 °C under N_2 atmosphere at a heating rate of 10 °C/min, (d) Repetitive cyclic voltammograms in 0.1 M n-Bu_4NPF_6 in CH_2Cl_2 solution at a scan rate of 100 mV/s.

pentamer with at least 80 % yield. Conversion from hydroquinone to soluble $BHBT_2$ pentamer via Williamson etherification, bromination and Suzuki coupling were thoroughly characterized with FTIR, ^{13}C and ^{1}H NMR spectroscopies. The presence of hexyloxy side chains in compound **1** is determined from the intense peaks at about 2936 cm^{-1} and 2871 cm^{-1} due to $\nu_{as}(-CH_2-)$ and $\nu_s(-CH_2-)$ of methylene ether moiety, respectively. These results are supported by the appearance of another two intense peaks at about 1239 cm^{-1} and 1032 cm^{-1} which attributed to $\nu_{as}(=COC-)$ and $\nu_s(=COC-)$ between phenylene and alkyloxy side chains. The stretching vibration of long linear aliphatic carbon chains were represented by peaks at about 1161 cm^{-1} and 1057 cm^{-1}.

A medium peak at 635 cm^{-1} is referred to the ν(C-Br) of halogenated dihexyloxy phenylene **2** and this indicated that bromination on compound **1** was successfully conducted by using bromine in acetic acid glacial solution (Fig. 1). The Br is placed in

para-position of compound **1** as evidenced from the medium peaks at about 849 cm^{-1} which attributed to =C-H out of plane deformation, δ_{oop}(=C-H) of 1,2,4,5-tetrasubstituted benzene moiety. The favorable coupling between compound **2** with 2-thiophene boronic acid to yield coupled product, **3** caused the peak at 635 cm^{-1} disappeared. Several medium peaks related to thiophene rings therefore can be seen in the range of 1343 – 1533 cm^{-1}, due to in-plane deformation of thiophene rings, δ_{ip}(C=C). The vibration modes of thiophene rings can be observed through the =C-H ring stretching correspondingly at about 3090 cm^{-1} while stretching vibration of =C-S in thiophene is found to vibrate at about 682 cm^{-1}.

Br is successfully inserted at the 5,5'-position of compound **3** by using NBS in THF solution as it is represented by peak at about 658 cm^{-1}, due to ν(C-Br) of halogenated thiophene endcapped dihexyloxy phenylene **4** (Fig. 1). Peaks corresponding to stretching vibration of long linear aliphatic carbon chains remained the same at about 1162 cm^{-1} and 1058 cm^{-1}. The extension of π-conjugated backbone by incorporating more thiophene rings into compound **4**, resulted a more rigid $BHBT_2$ pentamer. Thus, $BHBT_2$ pentamer displayed weak IR spectra as shown in Fig. 1. The well-coupled compound **4** with 2-thiophene boronic acids via Suzuki coupling is determined by disappearance of stretching vibration peak of halogenated thiophene, ν(C-Br) at about 658 cm^{-1} as shown in the IR spectra of intermediate compound and $BHBT_2$ pentamer (Fig. 1).

The interpretations are well supported by the ^{13}C and ^{1}H NMR spectroscopies where assignments of the peaks are illustrated in ^{13}C and ^{1}H NMR spectra of $BHBT_2$ pentamer (Fig. 2). ^{13}C NMR spectra revealed that aliphatic carbons in hexyloxy chains resonated in the range of δ_C 14.0 - 70.0 ppm (C_3-C_8). Carbons in methylene ether moiety of compound **1** which represented the well formed hexyloxy side chains Williamson etherification is found to resonate at about δ_C 68.9 ppm (C_3) and they appeared as triplet at peak about δ_H 3.91 ppm (H_b) in ^{1}H NMR spectra. Phenylene moiety of compound **1** consisted of 4 protons and they resonated at about δ_H 6.83 ppm. The insertion of bromine into *para*-position of compound **1** via bromination reaction caused 2 integrated protons in phenylene moiety disappeared and the presence of highly electronegative bromine tended to reduce electron density around the adjacent proton [14]. As a result, the remaining protons in phenylene moiety of compound **2** are found deshielded and then shifted downfield to δ_H 7.09 ppm. This was also supported by observation that brominated carbon in phenylene moiety resonated at δ_C 111.4 ppm.

Coupling of compound **2** with 2-thiophene boronic acid was well defined through the disappearance of brominated carbon peak at δ_C 111.4 ppm and additional new peaks appeared in the range of δ_C 123.1 – 139.3 ppm (C_9-C_{12}) due to the presence of thiophene rings in the coupled compound **3**. Coupling between phenylene dihexyloxy moiety, **2** with thiophene rings in compound **3** can be determined from the formation of two quaternary carbons which resonated correspondingly at δ_C 123.1 ppm (C_{2a}) and 139.3 ppm (C_9) (Fig. 3). The analysis and interpretation of compound **3** is based on previous reports [13, 20].

Carbons in the thiophene rings are represented by the resonance peaks at δ_C 125.2 (C_{10}), 126.7 (C_{11}) and 125.6 (C_{12}) ppm. This was supported by 2 integrated protons each at δ_H 7.35 (H_g), 7.11 (H_h) and 7.55 ppm ($H_{h'}$), respectively with $^{3}J_{Hg\text{-}Hh}$ 5.40 Hz and $^{3}J_{Hh\text{-}Hh'}$ 3.60 Hz. Bromination of compound **3** with NBS in THF solution successfully inserted the bromines on α and α'-position of thiophene rings. Brominated carbon in thiophene rings was found to resonate at δ_C 113.2 ppm as observed from ^{13}C NMR spectrum of compound **4**. Coupling between compound **4** with 2-thiophene boronic acid caused carbon peak at δ_C 113.2 ppm disappeared and replaced by two additional peaks in the range of δ_C 137.3-138.0 ppm due to the α-α' bonding between two thiophene rings [21]. Further analysis on ^{1}H NMR spectra found most of the protons in thiophene rings displayed doublet peaks with proton chemical shifts ranging from δ_H 7.03 – 7.46 ppm. The ^{13}C and ^{1}H NMR chemical shifts and assignment of the $BHBT_2$ pentamer was illustrated in Fig. 2.

Optical, thermal and electrochemical properties of $BHBT_2$ pentamer

The incorporation of compounds **2** with hexyloxy substituent is an important intermediate that can contribute to good solubility of 2,2'-bithiophene end-capped dihexyloxy-phenylene pentamer in common organic solvents such as tetrahydrofuran (THF), chloroform ($CHCl_3$) and dichloromethane (CH_2Cl_2) (Table 1). This is in good agreement with previous reports.[19, 22, 23] The improved solubility characteristic of $BHBT_2$ pentamer is due to the binding forces that holding the pentamer become weak as the presence of the branching dihexyloxy chains prevented self-aggregation among intermolecular [24].

The absorption maximum of $BHBT_2$ pentamer in chloroform exhibited two broad bands centered at 344 nm (3.60 eV) and 360 nm (2.98 eV), which related to π-π* transition between thiophene and bithiophene groups with 2,5-bis(dihexyloxy)benzene moiety in the π-conjugated backbone respectively. This indicated that the incorporation of terminal bithiophenes into 2,5-bis(dihexyloxy)benzene moiety allows greater charge transfer character in the π-conjugated backbones. The optical band gap, E_g which was estimated from the onset absorption edge and corrected baseline (Fig. 3a) ($Eg=1240/\lambda_{onset}$ eV) showed that $BHBT_2$ pentamer has an optical bandgap of 2.69 eV which found have an identical energy as polypara-phenylene (~2.7 eV). As referred to Fig. 3a, $BHBT_2$ pentamer in chloroform displayed two PL peaks at about 467 nm and 496 nm with the emission colour fall in the blue region (450-500 nm).

The first heating-cooling cycle in DSC thermogram was conducted to eliminate the thermal history of $BHBT_2$ pentamer before actual measurement was recorded on the second heating-cooling cycle (Fig. 3b). DSC thermogram in Fig. 3b exhibited a sharp endothermic peak with narrow half-width of melting ranging 1.6-2.2 °C. It revealed that the synthesized $BHBT_2$ pentamer was in pure condition. It was found that $BHBT_2$ pentamer melted nearly at 150 °C and this is comparable to the result measured from the melting

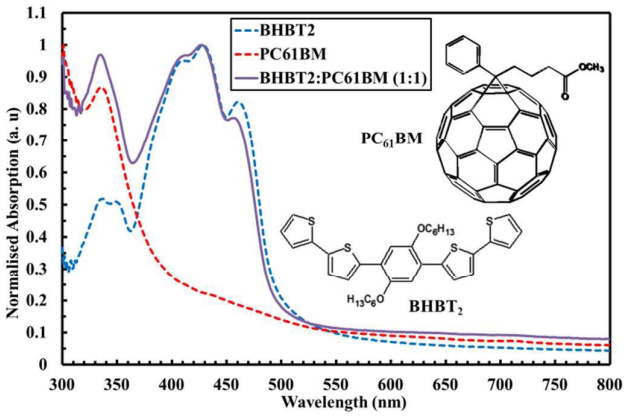

Fig. 4 Normalized absorption spectra of $BHBT_2$, $PC_{61}BM$ and $BHBT_2$:$PC_{61}BM$ thin films. (Inset) $BHBT_2$ and $PC_{61}BM$ molecular structure.

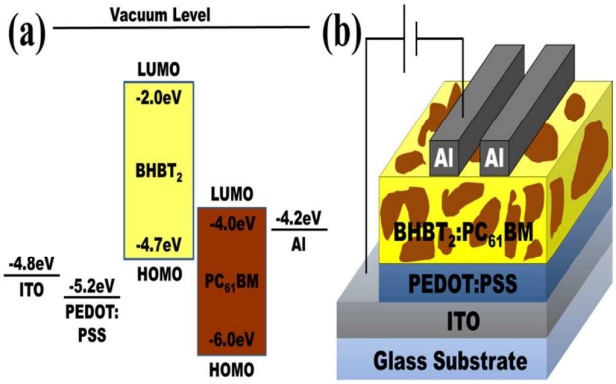

Fig. 5 (a) Energy level of the organic materials and work function of electrodes, (b) Schematic device structure of the organic UV photodetector.

point apparatus. No signs of polymorphism observed in the DSC thermogram of $BHBT_2$ pentamer and it showed that this pentamer underwent reversible enantiotropy where it remained stable in its actual form up to 200 °C. Upon cooling, $BHBT_2$ pentamer recrystallized at about 109.5 °C as indicated by the exothermic peak in Fig.1b which is found lower than the melting temperature, T_m, due to super cooling effect [25]. Further studies from the TGA thermogram results showed that $BHBT_2$ pentamer was thermally stable up to 307 °C before this material started to decompose. A loss of 10 % mass is observed in the derivative thermogravimetric curves (DTG) in a temperature range above 375 °C (Fig. 3c). A high thermal stability of $BHBT_2$ pentamer have assured this material suitable to be applied as an active layer in the devices processing which needed evaporation of materials below 200 °C.

The cyclic voltammetry (CV) was used to determine the oxidation potentials of $BHBT_2$ pentamer. The CV curves were measured in the range of 0 to +1.5 V (*vs.* SCE) at ambient temperature and calibrated using ferrocene/ferrocenium (Fc/Fc^+) redox couple as an external standard. The $E_{1/2}$ of the ferrocene was found to be 0.44 V versus the SCE quasi-reference electrode. The E_{ox} was obtained from the onset potential for oxidation relative to the SCE quasi-reference electrode in cyclic voltammetry while the optical band gap, E_g was estimated from the onset edge UV-vis absorption. Thus, the E_{HOMO} can be estimated via this empirical relation $E_{HOMO} = [(E_{ox} - E_{1/2(ferrocene)}) + 4.8]$ eV. E_{LUMO} was derived from the relationship of $E_{LUMO} = E_{HOMO} - E_g$.

As shown in Fig. 3d, cyclic voltammograms of $BHBT_2$ pentamer displayed three oxidation redox couples at 0.29 V ($E_{1/2(ox1)}$), 0.81 V ($E_{1/2(ox2)}$) and 1.07 V ($E_{1/2(ox3)}$), respectively. The onset oxidation potential of $BHBT_2$ pentamer started as low as 0.22 V. Thus, the calculated HOMO and LUMO energies from the voltammogram of $BHBT_2$ pentamer are correspondingly at ca. 4.65 eV and 1.96 eV with an optical bandgap of 2.69 eV as estimated from the absorption edge of the UV spectrum.

$BHBT_2$:$PC_{61}BM$ photodetector properties

Fig. 4 shows the normalized absorption spectra of $BHBT_2$, $PC_{61}BM$ and $BHBT_2$:$PC_{61}BM$ (ratio 1:1) blended thin films with their respective molecular structure. $BHBT_2$ thin film exhibited two strong UV absorption regions in the range of 315 nm to 360 nm with absorption maximum at 335 nm and a shoulder peak at 350 nm while the second absorption ranged within 360-500 nm where an absorption maximum at 430 nm and two shoulder peaks corresponded at 400 nm and 460 nm can be observed. This showed that $BHBT_2$ thin film possesses excellent absorption in the high-energy visible region (UV – blue). The $BHBT_2$:$PC_{61}BM$ blended thin film also displayed a similar absorption pattern as the $BHBT_2$ thin film, indicating that blending of $BHBT_2$ with $PC_{61}BM$ does not altered the chemical structures of the $BHBT_2$ and $PC_{61}BM$ in the bulk heterojunction system. $PC_{61}BM$ which have strong absorption in the short wavelength range (300 nm - 350 nm), helps to compensate the weak absorption of $BHBT_2$ in this region. Thus, $BHBT_2$:$PC_{61}BM$ blended thin film can contribute to photogeneration of the carriers in the complementary absorption spectra from 300 nm to 500 nm and make them prominence materials as UV detector. In addition, $PC_{61}BM$ is easily solution-processed and its high mobility (μ = 0.21 cm^2/Vs) characteristic is believed can helps to improve the performance of the fabricated UV photodetector. [9, 26]

Fig. 5a depicts the energy level of the materials used to fabricate the UV photodetector. The diagram shows that there is about 0.7 eV offset between the highest occupied molecular orbital (HOMO) of $BHBT_2$ (donor) and the lowest unoccupied molecular orbital (LUMO) of $PC_{61}BM$ (acceptor) at the D-A interface. The energy difference contributes to the formation of internal electric field which facilitates the dissociation of excitons (bound electron-pairs) besides governs the V_{oc} value of the photodetector. [27-31] Additionally, one can notices from this band diagram that the energy difference between LUMO offset of the donor and acceptor is large. This may cause a hurdle for the charge carriers to be transferred through percolating paths from the $BHBT_2$/PCBM interface to the electrodes. Consequently, low carriers recombination followed by charges accumulation in the system may

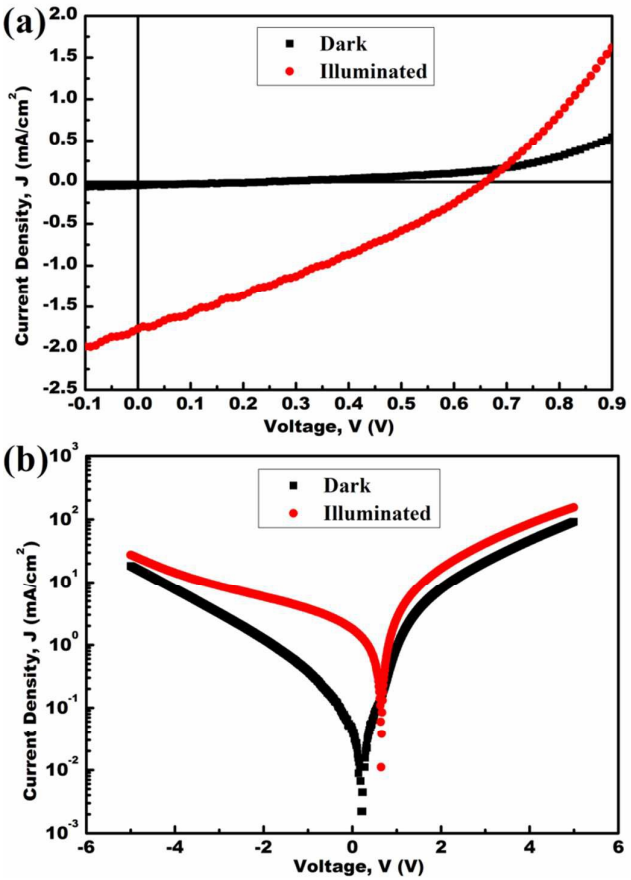

Fig. 6 (a) The current-voltage characteristics of ITO/PEDOT:PSS/$BHBT_2$:$PC_{61}BM$/Al photodetector under forward bias. (b) The logarithmic plot of J--V.

occurred, resulting a low V_{oc} value.[32]

The device structure of the photodetector is schematically shown in Fig. 5b. The photoactive layer of $BHBT_2$:$PC_{61}BM$ was sandwiched between a transparent indium tin oxide (ITO) anode and an aluminium (Al) cathode. Under reverse bias, the charges injection from the electrodes becomes the major source of dark current. Therefore, a thickness of (38±3) nm of PEDOT:PSS layer was inserted in between the photoactive layer and the ITO electrode to act as an electron blocking layer which functioned to minimize the dark current by reducing the charge carriers injection during reverse bias.[33]

The current-voltage (J-V) characteristics of ITO/PEDOT:PSS/$BHBT_2$:$PC^{61}BM$/Al photodetector under forward and reverse biases are depicted in Fig. 6. The photodetector is found to exhibit decent photovoltaic effect under 36 mW/cm^2 simulated sunlight by using AM 1.5 G solar illumination. The device showed a short-circuit current density, J_{sc} of 1.80 mA/cm^2 and open-circuit voltage, V_{oc} of 0.66 V. However, the achieved fill factor (FF) was merely 0.30 where it managed to generate a photovoltaic conversion efficiency (PCE) of 0.98 %. The rectification ratio (J_{ph}/J_{dark}) of the photodetector at zero applied voltage is found to be low as calculated 39.8. This indicates that the photodetector have

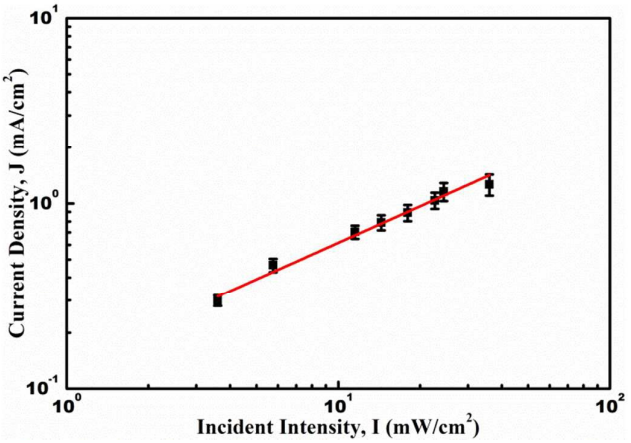

Fig. 7 Photosensitivity linearity measurement of ITO/PEDOT:PSS/$BHBT_2$:$PC_{61}BM$/Al photodetector.

Table 2 Photovoltaic properties of the UV photodetector when biased at 0 V under 36 mW/cm^2 AM 1.5 G solar illumination.

	J_{sc} (mA/cm^2)	V_{oc} (V)	FF	PCE (%)	Rectification Ratio
$BHBT_2$:$PC_{61}BM$	1.80	0.66	0.30	0.98	39.8

low shunt resistance which later affects the built-up potential in the system, possibly due to the presence of other short chain oligomers in $BHBT_2$ layer as seen in Fig.3b that expected disrupting the molecular arrangement in the pristine cell.

Moreover, the energy levels diagram as represented in Fig 5(a) showed that both $BHBT_2$ donor and $PC_{61}BM$ acceptor have large HOMO offset of 1.3 eV and LUMO offset of 2.0 eV, respectively. These large energy offsets may have caused difficulties for the dissociated electrons and holes to be transferred to their respective electrodes. The charge accumulation that subsequently occurred in the system further affected the efficiency of charge carriers' transportation and thus yielded a low J_{sc} value. In addition, there was 0.5 eV barrier from HOMO level of $BHBT_2$ to the PEDOT:PSS and the presence of this large barrier further obstructed the transportation of holes to the ITO electrode.

Besides large energy offset between $BHBT_2$ donor and $PC_{61}BM$ acceptor, active layer thickness is expected to play yet another important role behind the low gain of this UV photodetector. The short singlet exciton diffusion length (~10 nm)[34-36] has constrained organic electronics active layers to thicknesses ranging from 60 nm to 130 nm. Therefore, there are two possible consequences for the excitons in $BHBT_2$:$PC_{61}BM$ active layer with thickness of about 180 nm as prepared in this work. The excitons may have undergone charge recombination before reaching the donor–acceptor interfaces or some excitons survived from charge recombination and managed to diffuse to their respective electrodes for active layer thicker than 130 nm. However, the performance of this photodetector displayed a decrease of generated J_{sc} due to affected hole mobility leading to higher charge carrier recombination rate. This observation is very much in accordance with literature where

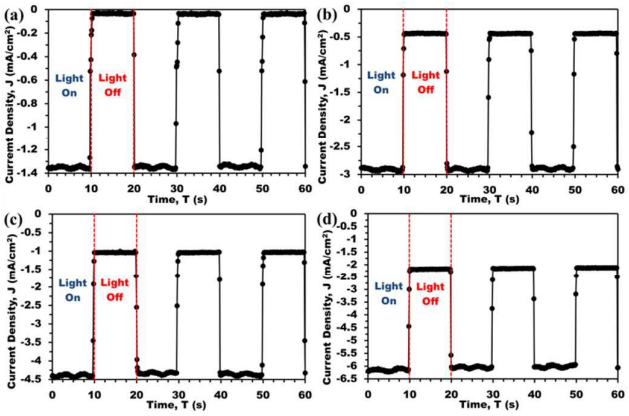

Fig. 8 The cyclic performance or time response measurement of ITO/PEDOT:PSS/ $BHBT_2$:$PC_{61}BM$/Al photodetector when biased at (a) 0 V, (b) -1 V, (c)-2 V and (d)-3 V under on/off modulation (irradiation intensity of 36 mW/cm^2).

absorber layers thicker than 130 nm are often reported as inefficient factor for many organic electronics.[37-39] Thickness optimization can be carried out in order to enhance the performance of the organic UV PDs. Moreover, the performance of this photodetector probably can be further improved by undergoes post fabrication annealing at higher temperature to provide better molecular ordering.[40] The dark current density under zero bias is found to be nearly 50 μA/cm^2. By comparing the dark and illuminated J-V curves, the highest gain of this detector is about two orders in magnitude if operated at 0.2 V as the lowest dark current density appeared at this voltage instead of at 0 V. Table 2 summarizes the photovoltaic parameters and efficiency of the photodetector at zero-applied voltage under 36 mW/cm^2 AM 1.5 G solar illumination.

The photocurrent density versus the input light intensity for the photodetector is represented in Fig. 7. This measurement was conducted to examine the photosensitivity linearity and used to determine the limit of the photodetector operation. It is observed that the photocurrent density of the photodetector responses linearly to the incident intensity ranged from 3.6 - 36 mW/cm^2 at zero-bias voltage.

The photoresponse of the $BHBT_2$:$PC_{61}BM$ photodetector is explored by adapting the transient photocurrent study. Transient photocurrent measurement was performed by biasing a constant potential across the device while pulsing the light to the device. The photocurrent of the photodetector is observed increasing sharply when irradiated under negative bias. This followed by photocurrent remained nearly constant during the periods of illumination. After switched off the light, the photocurrent of the device returned back to its initial value and remained relatively stable. As shown in Fig. 8, the cyclic performance of $BHBT_2$:$PC_{61}BM$ photodetector exhibited fast and stable on/off switching when biased correspondingly at 0 V, -1 V, -2 V and -3 V under 36 mW/cm^2 on/off modulation. It showed exceptional reproducibility without considerable variation to demonstrate its good stability.

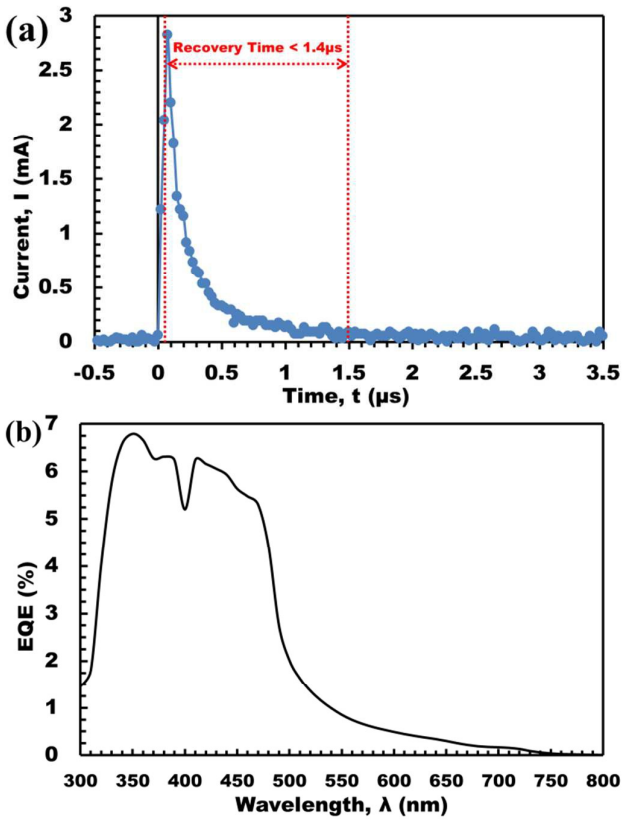

Fig. 9 (a) Transient photocurrent measurement for ITO/PEDOT:PSS/$BHBT_2$:$PC_{61}BM$/Al photodetector at 0 V bias under 20 Hz of 337 nm laser pulse, (b) The external quantum efficiency (EQE) of the ITO/PEDOT:PSS/$BHBT_2$:$PC_{61}BM$/Al photodetector.

The gain (on/off ratio) of the device was derived according to the equation of gain = J_{ph}/J_{dark} and was determined under various negative biases. The highest gain is found located at zero-applied voltage and subsequently declined when approaching higher negative voltages. This phenomenon is observed in Fig. 8 where the gaps between J_{dark} and J_{ph} became smaller when higher negative bias was applied on the photodetector. It is expected that the charges injection become greater at higher reverse bias, causing the rise of the dark current density and thus reducing the gain obtained. As shown in Fig. 6b, the dark current at the reverse bias continued increasing during higher negative voltage applied on the photodetector. With assumption that the shot noise from the dark current is the major contribution to the noise, the detectivity, D^* is expressed as $D^*=(J_{ph}/L_{light})/(2qJ_{dark})^{1/2}$, where L_{light} is the incident light intensity and q is the absolute value of electron charge (1.6 × 10^{-19} coulombs).[10, 16, 33, 41-43] At zero-applied voltage, the photodetector is determined to have the highest detectivity of 1.47 × 10^9 Jones under an incident intensity of 36 mW/cm^2.

Further investigation was done to determine the fast response properties of ITO/PEDOT:PSS/$BHBT_2$:$PC_{61}BM$/Al photodetector. Transient photocurrent was recorded through pulsing 337 nm laser pulses (3 ns pulse width) with the rate of 20 Hz on the photodetector. Fig. 9 (a) shows the photoresponse characteristics

of the photodetector at 0 V. It is found that the device displayed a very short recovery time when triggered by the UV laser pulse. The rise time is less than 0.1 μs after trigged and the decay time is less than 1.4 μs after irradiation was turned off. The response times of the photodetector is found faster than those reported for a vertically stacked bulk heterojunction organic photodetector (<200 ms)[12], an inverted stacked structure organic UV photodetector (<200 ms)[16], an planar structured organic photodetector (<20 ms)[44] as well as for an organic-inorganic hybrid structured photodetector (~21 ms)[41]. Fast response speed and short recovery time are important for photodetector because the response time determined the bandwidth available for signal modulation where it presented the data transmission in an optical communication system.[45]

The external quantum efficiency (EQE) of the ITO/PEDOT:PSS/$BHBT_2$:$PC_{61}BM$/Al photodetector that represents fraction of survival photoexcitations from charge separation and successfully to reach the electrodes through percolation paths is shown in Fig. 10. The deep valley that appeared at around 400 nm (Fig. 9 (b)) is due to the switching light source of the EQE measurement system. The EQE spectrum is found to display similar curve as UV absorption spectrum of the $BHBT_2$:$PC_{61}BM$ blended thin film (Fig. 4) and this explains that most of the light harvesting activity of the photodetector takes place at the wavelength range of 300 nm to 500 nm. In spite of low EQE percentage (~ 7%) achieved by this photodetector that resulted poor performance in solar cell application especially with low FF value (FF=0.3) but this device is still competent for photodetector applications. As a result, the photodetector based on $BHBT_2$:$PC_{61}BM$ bulk heterojunction showed sufficient light harvesting characteristic in the UV region, thus making them promising candidates for organic UV photodetector.

Conclusions

In summary, we have designed a small molecular donor based on thiophene-phenylene oligomer which has good solubility in common organic solvents, due to the presence of dihexyloxy benzene moiety. The incorporation of dihexyloxy benzene moiety in 2,2'-bithiophene end-capped dihexyloxy phenylene pentamer ($BHBT_2$) helps to surpass the solubility limits of typical unsubstituted oligomers. The yielded $BHBT_2$ pentamer was highly pure with certain degree of crystalline region as shown in the DSC thermograms and was thermally stable up to 307 °C. This small molecular donor has an identical optical bandgap, E_g (ca. 2.69 eV) as polypara-phenylene with HOMO and LUMO energies at 4.65 eV and 1.96 eV, respectively.

The advantage of soluble $BHBT_2$ allowed this donor material can be prepared in solution processed photodetector in conjunction with $PC_{61}BM$ as acceptor material. The $BHBT_2$:$PC_{61}BM$ heterojunction layer displayed strong absorption in the UV region from 300 nm to 500 nm as a result of complementary absorption from $BHBT_2$ and $PC_{61}BM$, respectively. The utilization of $PC_{61}BM$, greatly enhanced the optical absorption in the UV regime and thus improved the electrical performance of the photodetectors. This has made the $BHBT_2$:$PC_{61}BM$ good combination materials for UV range photodetector. The ITO/PEDOT:PSS/$BHBT_2$:$PC_{61}BM$/Al photodetector responded linearly to the incident intensity from 3.6 mW/cm^2 to 36 mW/cm^2 at zero-applied voltage. Under illumination intensity of 36 mW/cm^2 at 0 V, the photodetector exhibited reversible, stable and fast response time with the highest detectivity of 1.47×10^9 Jones.

Acknowledgements

This research was financially supported by High Impact Research MoE Grant UM.S/625/3/HIR/MoE/SC/26 from the Ministry of Education Malaysia and Postgraduate Research (PPP) Grant (project no. PG053-2015B) from the University of Malaya. The authors also acknowledge Universiti Kebangsaan Malaysia (UKM) for their financial supports via grant UKM-GUP-BTT-07-26-178. The authors also like to thank Dr. C.C. Yap from Universiti Kebangsaan Malaysia for providing the EQE systems and valuable discussions.

Notes and references

1. Z. Su, F. Hou, X. Wang, Y. Gao, F. Jin, G. Zhang, Y. Li, L. Zhang, B. Chu and W. Li, *ACS Applied Materials & Interfaces*, 2015, **7**, 2529-2534.
2. N. M. Kronenberg, M. Deppisch, F. Wurthner, H. W. A. Lademann, K. Deing and K. Meerholz, *Chemical Communications*, 2008, 6489-6491.
3. J. L. Segura, N. Martin and D. M. Guldi, *Chemical Society Reviews*, 2005, **34**, 31-47.
4. F. Lefèvre, P. Juneau and R. Izquierdo, *Sensors and Actuators B: Chemical*, 2015, **221**, 1314-1320.
5. J.-r. Lian, Y.-b. Yuan, L.-f. Cao, J. Zhang, H.-q. Pang, Y.-f. Zhou and X. Zhou, *Journal of Luminescence*, 2007, **122–123**, 660-662.
6. Y. Shen, X. Yan, Z. Bai, X. Zheng, Y. Sun, Y. Liu, P. Lin, X. Chen and Y. Zhang, *RSC Advances*, 2015, **5**, 5976-5981.
7. W. Dai, X. Pan, S. Chen, C. Chen, W. Chen, H. Zhang and Z. Ye, *RSC Advances*, 2015, **5**, 6311-6314.
8. F. Meng, L. Shen, Y. Wang, S. Wen, X. Gu, J. Zhou, S. Tian and S. Ruan, *RSC Advances*, 2013, **3**, 21413-21417.
9. H. Lee, S. Nam, H. Kwon, S. Lee, J. Kim, W. Lee, C. Lee, J. Jeong, H. Kim and T. J. Shin, *Journal of Materials Chemistry C*, 2015, **3**, 1513-1520.
10. X. Gong, M. Tong, Y. Xia, W. Cai, J. S. Moon, Y. Cao, G. Yu, C.-L. Shieh, B. Nilsson and A. J. Heeger, *Science*, 2009, **325**, 1665-1667.
11. S.-h. Wu, W.-l. Li, B. Chu, C. S. Lee, Z.-s. Su, J.-b. Wang, F. Yan, G. Zhang, Z.-z. Hu and Z.-q. Zhang, *Applied Physics Letters*, 2010, **96**, 093302.
12. H.-G. Li, G. Wu, H.-Z. Chen and M. Wang, *Current Applied Physics*, 2011, **11**, 750-754.
13. P. Data, M. Lapkowski, M. Motyka and J. Suwinski, *Electrochimica Acta*, 2012, **83**, 271-282.
14. R. M. Silverstein and F. X. Webster, in *Spectrometric identification of organic compounds.*, John Wiley & Sons, USA, Editon edn., 1998.

15. C.-B. Liu, M. Liu, G.-B. Che, B. Su, L. Wang, X.-X. Zhang and S. Zhang, *Solid-State Electronics*, 2013, **89**, 68-71.
16. X. Wang, H. Wang, W. Huang and J. Yu, *Organic Electronics*, 2014, **15**, 3000-3005.
17. W. L. F. Armarego and C. L. L. Chai, *Purification of Laboratory Chemicals*, 5th edn., Elsevier Science, Oxford, 2003.
18. B. A. Reinhardt, L. L. Brott, S. J. Clarson, A. G. Dillard, J. C. Bhatt, R. Kannan, L. X. Yuan, G. S. He and P. N. Prasad, *Chemistry of Materials*, 1998, **10**, 1863-1874.
19. S. P. Huang, G. S. Huang and S. A. Chen, *Synth. Met.*, 2007, **157**, 863-871.
20. V. Promarak and S. Ruchirawat, *Tetrahedron*, 2007, **63**, 1602.
21. M. Lanzi, L. Paganin and D. Caretti, *Polymer*, 2008, **49**, 4942-4948.
22. J. P. Lere-Porte, J. J. E. Moreau, F. Serein-Spirau, C. Torreilles, A. Righi, J. L. Sauvajol and M. Brunet, *J. Mater. Chem.*, 2000, **10**, 927-932.
23. C. C. Ho, K. M. Yeh and Y. Chen, *Polymer*, 2004, **45**, 8739.
24. A. R. Katritzky, R. Jain, A. Lomaka, R. Petrukhin, U. Maran and M. Karelson, *Cryst. Growth Des.*, 2001, **1**, 261-265.
25. J. I. Pak, M. Pyda and B. Wunderlich, *Thermochimica Acta*, 2003, **396**, 43-56.
26. P. H. Wöbkenberg, D. D. C. Bradley, D. Kronholm, J. C. Hummelen, D. M. de Leeuw, M. Cölle and T. D. Anthopoulos, *Synthetic Metals*, 2008, **158**, 468-472.
27. S. Günes, H. Neugebauer and N. S. Sariciftci, *Chemical Reviews*, 2007, **107**, 1324-1338.
28. C. J. Brabec, A. Cravino, D. Meissner, N. S. Sariciftci, T. Fromherz, M. T. Rispens, L. Sanchez and J. C. Hummelen, *Advanced Functional Materials*, 2001, **11**, 374-380.
29. J. Hou, C. Yang, J. Qiao and Y. Li, *Synthetic Metals*, 2005, **150**, 297-304.
30. C. Liu, L. Liu, G. Che, Y. Cui, Q. Wang, W. Li and M. Liu, *Solar Energy Materials and Solar Cells*, 2012, **96**, 29-32.
31. Y. Cui, L. Liu, C. Liu, Q. Wang, W. Li, G. Che, C. Xu and M. Liu, *Synthetic Metals*, 2010, **160**, 373-375.
32. G. T. Mola and N. Abera, *Physica B*, 2014, **445**, 56-59.
33. C. Chi Hang, K. Do Young, J. Subbiah, C. M. Amb, J. R. Reynolds and F. So, *Electron Devices, IEEE Transactions on*, 2014, **61**, 3852-3857.
34. Y. Tamai, H. Ohkita, H. Benten and S. Ito, *The Journal of Physical Chemistry Letters*, 2015, **6**, 3417-3428.
35. C. Leow, T. Ohnishi and M. Matsumura, *The Journal of Physical Chemistry C*, 2014, **118**, 71-76.
36. R. R. Lunt, N. C. Giebink, A. A. Belak, J. B. Benziger and S. R. Forrest, *Journal of Applied Physics*, 2009, **105**, 053711.
37. J. Mescher, A. Mertens, A. Egel, S. W. Kettlitz, U. Lemmer and A. Colsmann, *AIP Advances*, 2015, **5**, 077188.
38. F. Nickel, C. Sprau, M. F. G. Klein, P. Kapetana, N. Christ, X. Liu, S. Klinkhammer, U. Lemmer and A. Colsmann, *Solar Energy Materials and Solar Cells*, 2012, **104**, 18-22.
39. M.-S. Kim, B.-G. Kim and J. Kim, *ACS Applied Materials & Interfaces*, 2009, **1**, 1264-1269.
40. A. C. Mayer, M. T. lloyd, D. J. Herman, T. G. Kasen and G. G. Malliaras, *Applied Physics Letters*, 2004, **85**, 6272-6274.
41. D. Shao, M. Yu, H. Sun, G. Xin, J. Lian and S. Sawyer, *ACS Applied Materials & Interfaces*, 2014, **6**, 14690-14694.
42. Y. J. Kim, C. E. Park and D. S. Chung, *Physical Chemistry Chemical Physics*, 2014, **16**, 18472-18477.
43. B. T. Lim, I. Kang, C. M. Kim, S. Y. Kim, S.-K. Kwon, Y.-H. Kim and D. S. Chung, *Organic Electronics*, 2014, **15**, 1856-1861.
44. K.-J. Baeg, M. Binda, D. Natali, M. Caironi and Y.-Y. Noh, *Advanced Materials*, 2013, **25**, 4267-4295.
45. T. Morimune, H. Kajii and Y. Ohmori, *Photonics Technology Letters, IEEE*, 2006, **18**, 2662-2664.